PCCP

PAPER

View Article Online
View Journal | View Issue

Cite this: *Phys. Chem. Chem. Phys.*, 2017, **19**, 10685

Synthesis, structure and bonding of actinide disulphide dications in the gas phase†

Ana F. Lucena,[a] Nuno A. G. Bandeira,*[bcd] Cláudia C. L. Pereira,‡[a] John K. Gibson[e] and Joaquim Marçalo*[a]

Received 7th March 2017,
Accepted 5th April 2017

DOI: 10.1039/c7cp01446e

rsc.li/pccp

Actinide disulphide dications, AnS_2^{2+}, were produced in the gas phase for An = Th and Np by reaction of An^{2+} cations with the sulfur-atom donor COS, in a sequential abstraction process of two sulfur atoms, as examined by FTICR mass spectrometry. For An = Pu and Am, An^{2+} ions were unreactive with COS and did not yield any sulphide species. High level multiconfigurational (CASPT2) calculations were performed to assess the structures and bonding of the new AnS_2^{2+} species obtained for An = Th, Np, as well as for An = Pu to examine trends along the An series, and for An = U to compare with a previous experimental study and DFT computational scrutiny of US_2^{2+}. The CASPT2 results showed that, like in the case of uranium, the new AnS_2^{2+} ions have ground states with triangular geometries, corresponding to the presence of a persulphide in the case of thorium that formally leads to a stable $Th^{IV}S_2^{2+}$ species, while a supersulphide appears to be present in the case of U, Np and Pu, formally leading to a $An^{III}S_2^{2+}$ species. The computations also revealed that linear thioactinyl structures are higher in energy, with a difference that increases fourfold upon moving from U to Pu, apparently indicating that it will be even more pronounced for Am.

Introduction

The actinyl dications, $An^{VI}O_2^{2+}$, are especially significant in the chemistry of U, Np, Pu, and Am.[1] Uranyl in particular has received widespread consideration from both the experimental and theoretical perspectives.[2–10] The synthesis of analogues of uranyl, where oxygen is replaced by another main-group element or moiety, such as carbene, imido, and terminal chalcogenide, has multiplied in recent years and is still an ongoing endeavour.[11–15] For the less-studied transuranium actinides, only recently has a first actinyl V or VI analogue been successfully prepared, specifically a *trans*-bisimido complex of Np(v).[16]

A particular goal has been to synthesize species that integrate bonds between uranium and sulphur, the closest chalcogenide homologue of oxygen, namely thiouranyl, US_2^{2+}.[14,17] We recently reported a detailed study of the gas-phase reactions of monopositive and dipositive uranium cations with COS, with focus on the formation of US_2^{2+}, potentially the thiouranyl ion.[18] Remarkably, density functional theory (DFT) computations indicated that the ground-state structure for this species is triangular US_2^{2+}, with a side-on η^2-S_2 ligand, while the linear thiouranyl isomer, $\{S{=}U{=}S\}^{2+}$, was computed to be 40.9 kcal mol^{-1} higher in energy.[18]

In actinide chemistry, the issue of the extent of covalency in metal–ligand interactions has been pervasive and long lasting.[19–22] Molecules involving metal–ligand interactions with multiple-bond character are strong indicators of the extent of

[a] *Centro de Ciências e Tecnologias Nucleares, Instituto Superior Técnico, Universidade de Lisboa, 2695-066 Bobadela LRS, Portugal. E-mail: jmarcalo@ctn.tecnico.ulisboa.pt*
[b] *Institute of Chemical Research of Catalonia (ICIQ), Barcelona Institute of Technology (BIST), 16 – Av. Països Catalans, 43007 Tarragona, Spain. E-mail: nbandeira@iciq.es*
[c] *Centro de Química Estrutural, Instituto Superior Técnico, Universidade de Lisboa, Av. Rovisco Pais 1, 1049-001 Lisboa, Portugal*
[d] *Centro de Química e Bioquímica, Faculdade de Ciências, Universidade de Lisboa, Campo Grande, 1749-016 Lisboa, Portugal*
[e] *Chemical Sciences Division, Lawrence Berkeley National Laboratory, Berkeley, California 94720, USA*

† Electronic supplementary information (ESI) available: Experimental details; reaction products and kinetics for the reactions of AnS_2^{2+} and AnS_3^{2+} with COS; calculated geometries of the ground states of di-haptic actinide disulphides: η^2-ThS_2^{2+} (MP2), η^2-US_2^{2+} [CASPT2(4,8)], η^2-NpS_2^{2+} [CASPT2(5,8)] and η^2-PuS_2^{2+} [CASPT2(6,8)]; main data from the CASPT2(4,8) optimisation of η^2-UO_2^{2+}; main data from the CASPT2(13,13) single point calculation of η^2-NpS_2^{2+}; MO composition of the main bonding orbitals in η^2-AnS_2^{2+} extracted from the corresponding CASPT2(n,13) wavefunction; active space MOs used in the energy calculation of triangular species, such as η^2-NpS_2^{2+}, used in the CASPT2(13,13) calculations; Mayer Bond Order (MBO) values of each ground state geometry calculated with the CASPT2(n,13) method; MO symmetry species and corresponding axis frame definition used in the symmetry constrained calculations; CASPT2(n,13) energies (a.u.) of the symmetrised (C_{2v}) minima in each spin class with respective term symbols; state relative energies for each isomer class in $[SAnS]^{2+}$ and η^2-$[AnS_2]^{2+}$ cations (An = Np, Pu). All calculation outputs are available at the iochem-bd database and accessible at the following link: http://dx.doi.org/10.19061/iochem-bd-1-30. See DOI: 10.1039/c7cp01446e

‡ Present address: REQUIMTE, Faculdade de Ciências e Tecnologia, Universidade Nova de Lisboa, 2829-516 Caparica, Portugal.

covalency, and changes along the actinide series can be particularly illuminating. Therefore, in the present work, gas-phase studies of the formation of actinide disulphide dications were performed through reactions of An^{2+} ions with COS, for An = Th, Np, Pu, and Am, to complement previous studies with uranium and evaluate potential trends along the actinide series. Thorium was included in this study as reference, because it can only achieve a maximum oxidation state of +4 and cannot form actinyl or analogue species. Gas-phase ion-chemistry studies are generally conducted in combination with computational studies so that experimentally observed species can be elucidated. Here, we have opted for using high-level multiconfigurational (CASPT2) calculations to assess the structure and bonding of observed and non-observed AnS_2^{2+} species, and try to illuminate any trends for the early actinides.

There are very few reported studies on elementary molecular actinide disulphides. Andrews and co-workers accomplished the production of the neutral ThS_2 and US_2 by the reaction of sulphur vapour with laser-ablated metal atoms in cryogenic matrices.[23–25] In a previous study of An sulphides, we were able to produce AnS_2^+ ions for An = Th, Pa, U, and Np by sequential reactions of An^+ ions with OCS.[26] Earlier experiments by Gibson had shown that AnS_2^+ could be obtained using thiols as reagents for An = U, Np, Pu, and Am.[27]

Experimental details

Gas-phase experiments were performed by Fourier transform ion-cyclotron resonance mass spectrometry (FTICR-MS), using procedures described in detail in our previous studies of actinide sulphides,[18,26] as well as in the ESI.† The An^{2+} ions were produced by direct laser desorption/ionization of small pieces of alloys that contained ~20% of Th or ~5% of the remaining actinide metals (Np, Pu, Am) in a Pt matrix. The COS reagent, a commercial product with >99% purity as confirmed by electron ionization mass spectra, was introduced into the spectrometer through a leak valve to constant pressures of $(1–3) \times 10^{-7}$ Torr. The reactant An^{2+} ions or sequential product ions were isolated and product ion intensities were monitored as a function of the reaction time. The reactant ions were thermalized by collisions with argon, maintained at constant pressures in the range of $(1–5) \times 10^{-6}$ Torr. Rate constants, k, were determined from the pseudo-first-order decay of the relative signals of the reactant ions as a function of time at constant neutral pressures. Reaction efficiencies are described as k/k_{COL}, where the k_{COL} is the collisional rate constant (see the ESI†).

Computational details

Complete active space self-consistent field (CASSCF)[28,29] calculations were performed using the MOLCAS 8.0 package[30] to generate a reference space (CAS[n,m]), which consists of n electrons in the m molecular orbitals that describe the essential static correlation of the zeroth order wavefunction. All atoms were described with Atomic Natural Orbital[31] basis sets of the relativistic core contracted (ANO-RCC[32–34]) type. These calculations involved a default atomic mean field integral[35] (AMFI) computation with a second-order Douglas–Kroll–Hess Hamiltonian (DKH2).[36,37] The following contraction schemes were used: for Th, 27s24p18d14f6g3h → 9s8p6d4f2, for U, Np and Pu, 26s23p17d13f5g3h → 9s8p6d4f2g, and 17s12p5d → 4s3p1d for S. CASPT2 numerical gradients were performed without symmetry constraints to obtain stationary points on the lowest energy root within each multiplicity starting from a previously B3LYP optimised guess of the highest spin state of every system. Convergence thresholds were set to 10^{-3} and 10^{-6} a.u. for coordinate and gradient change respectively. The Cholesky[38] integral decomposition technique was chosen to speed up the optimisations. The default IPEA value of 0.25 a.u. was used for the zeroth order wavefunction in perturbative calculations. An imaginary level shift of 0.1 a.u. was imposed in the CASPT2 stage to alleviate the intruder state problem.

The triangular η^2-AnS_2^{2+} species underwent a CASPT2(4,8) (An = U), CASPT2(5,8) (An = Np) and CASPT2(6,8) (An = Pu) state specific geometry optimisation for every spin state. The linear ThS_2^{2+} and US_2^{2+} species are closed shell with a significant HOMO–LUMO gap so an optimisation at the CASPT2 level becomes unnecessary. Therefore, for computational efficiency, an MP2 optimisation was performed on these diamagnetic species and the CASPT2 calculations run on top of the optimised geometry. As is the case with active spaces with many doubly occupied or empty MOs (NOOs > 1.98, NOOs < 0.06) some inactive or external MOs outside of our model space intruded the CAS. To keep the correlation treatment consistent a rotation constraint was imposed on these intruder orbitals to maintain them outside the CAS *via* the Supsym keyword. This produced only a slight change in the final PT2 energy and a very small decrease in the weight of the zeroth order wavefunction of the perturbed solution. The An = U, Np, Pu linear cations underwent geometry optimisations that included all the bonding and anti-bonding combinations of the 3p orbitals. A single point evaluation with the same n,13 active space run on the remainder of all η^2-AnS_2^{2+} isomers to assess the linearization energies.

Symmetrised models of each stationary point underwent a single point CASPT2(n,13) run with C_{2v} symmetry in order to obtain the ground state term symbol of each model in this point group (see ESI†).

Results and discussion

Gas-phase synthesis of actinide disulphide dications

Gas-phase reactions of dipositive actinide cations, An^{2+} (An = Th, Np, Pu, Am), with COS were examined by FTICR-MS, with a focus on the formation of disulphide dications, AnS_2^{2+}, and for comparison with the previously studied U^{2+}.[18] As in the case of uranium, carbonyl sulfide was selected because it is a thermodynamically favorable sulfur-atom donor (D(OC–S) = 73.6 ± 0.2 kcal mol^{-1} and D(O–CS) = 160.6 ± 0.5 kcal mol^{-1} [39]) and also because it has a rather high ionization energy (IE(COS) = 11.18 eV[39]) that could disfavor electron-transfer pathways in the reactions with An^{2+} ions.

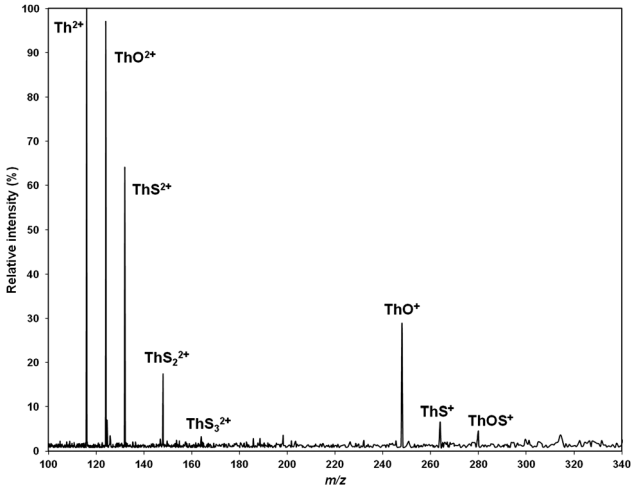

Fig. 1 Mass spectrum for the reaction Th^{2+} + COS (t = 0.1 s, P_{COS} = 2.0 × 10^{-7} Torr; P_{Ar} ~ 2 × 10^{-6} Torr).

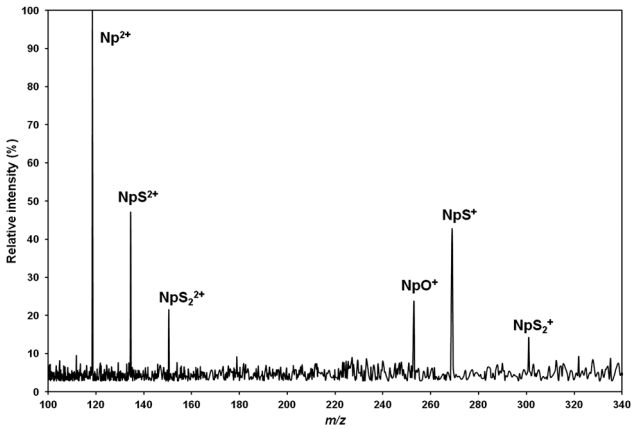

Fig. 2 Mass spectrum for the reaction Np^{2+} + COS (t = 0.2 s, P_{COS} = 2.5 × 10^{-7} Torr; P_{Ar} ~ 2 × 10^{-6} Torr).

AnS_2^{2+} ions were produced for An = Th and Np in a sequential abstraction process of two sulfur atoms by the An^{2+} ions, similarly to what was previously observed for U^{2+}.[18] For An = Pu and Am, An^{2+} ions were unreactive with COS (within the detection limit, $k/k_{COL} \leq 0.005$) and did not yield any sulphide species. Fig. 1 and 2 show representative mass spectra obtained in the reactions of Th^{2+} and Np^{2+}, respectively.

Table 1 summarizes the product distributions, rate constants and efficiencies for primary (An^{2+}) and secondary (AnS^{2+}) reactions with COS; the results previously obtained for the case of uranium are included for comparison. The reaction efficiencies of the An^{2+} cations followed the order: $Th^{2+} > U^{2+} > Np^{2+} \gg Pu^{2+} \approx Am^{2+} \approx 0$, a reactivity trend that has been observed before in the reactions of An^{2+} cations with other neutral molecules, namely oxidants and hydrocarbons.[40,41] Besides AnS^{2+}, primary formation of AnO^{2+} was observed for Th (and U) but not for Np; these results are in accord with $D(An^{2+}–O) > D(O–CS)$ for Th (and U) but not for Np.[42] Interestingly, the reaction efficiencies of the primary AnS^{2+} ions followed the order: $Np^{2+} > U^{2+} > Th^{2+}$.

Table 1 Reaction products and kinetics for the reactions of An^{2+} and AnS^{2+} with COS[a]

Reactant ion	Products	k/k_{COL} [k]	Reactant ion	Products	k/k_{COL} [k]
Th^{2+}	ThS^{2+} (25%) ThO^{2+} (60%) ThO^{+} (15%)	0.90 [1.75]	ThS^{2+}	ThS_2^{2+} (85%) ThS^{+} (15%)	0.67 [1.29]
U^{2+}	US^{2+} (60%) UO^{2+} (30%) UO^{+} (10%)	0.75 [1.45]	US^{2+}	US_2^{2+} (60%) US^{+} (20%) UO^{+} (20%)	0.79 [1.50]
Np^{2+}	NpS^{2+} (100%)	0.44 [0.85]	NpS^{2+}	NpS_2^{2+} (45%) NpS^{+} (55%)	0.92 [1.78]

[a] Where more than one product was observed, the relative yields are given in parentheses; the pseudo-first-order rates are expressed as reaction efficiencies, k/k_{COL}, and in brackets as absolute rates, $k/10^{-9}$ cm^3 molecule^{-1} s^{-1}; the data for uranium are from ref. 18.

As observed previously for uranium,[18] the new AnS_2^{2+} ions (An = Th, Np) reacted further with COS to form AnS_3^{2+} species. The reaction of ThS_3^{2+} could also be examined and, like uranium, yielded the tetrasulphide, ThS_4^{2+}, while the reaction of NpS_3^{2+} could not be studied due to poor ion signal. Details on these reactions (product distributions and kinetics) are presented in the ESI† (Table S1).

To summarize the experimental results, new actinide disulphide dications, AnS_2^{2+}, could be effectively prepared for An = Th and Np. However, gas-phase synthesis of a species with a specific composition and charge does not directly reveal structure and bonding. In our previous study of uranium sulphide cations,[18] DFT computations indicated that the ground state of the US_2^{2+} ion has a triangular structure, with the linear thiouranyl isomer 40.9 kcal mol^{-1} higher in energy. For the produced ThS_2^{2+} ion, the scenario should be different, as Th can only achieve a maximum oxidation state of +4, and, therefore, the formation of a stable Th^{IV} persulphide can be anticipated. For the case of NpS_2^{2+}, it is possible that a linear thioneptunyl is produced or, like in the case of US_2^{2+}, a triangular species with a side-on η^2-S_2 ligand. To assess the structure and bonding of the new AnS_2^{2+} species obtained for An = Th, Np, as well as for An = Pu to uncover trends along the An series, and for An = U to complement the previous study by DFT,[18] we performed CASSCF computations that are presented in the following section.

Structure and bonding of actinide disulphide dications

Since the crystal field of the 5f orbital environment in the actinide dications – herein they shall be named $5f_\sigma$, $5f_{\pi1}$, $5f_{\pi2}$, $5f_{\delta1}$, $5f_{\delta2}$, $5f_{\phi1}$, $5f_{\phi2}$ (see Fig. 3 below and ESI† for their representation) – produces very small splittings, the degree of static correlation will be significant and the high symmetry of these species will render it difficult or unreliable the use of single determinant methods such as DFT to reproduce the electronic structure of these species. Moreover, the small size of the systems is an advantage from a computational perspective and as such we performed a perturbative wavefunction geometry optimisation and analysis of actinide disulphide dications, AnS_2^{2+}. Pre-trials were conducted to assess the most

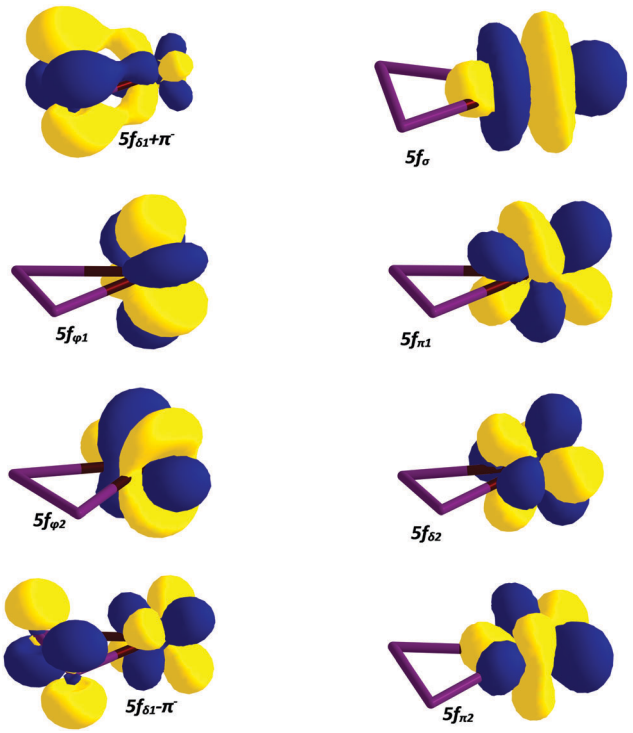

Fig. 3 Active space orbitals used for the geometry optimisation of the ground states of di-haptic actinide disulphides. Shown here are those of the ^{3}X state of η^2-US$_2^{2+}$.

adequate active space for the triangular and linear species. For the An = U, Np, Pu linear species, optimisations were performed at the CASPT2(12,13) and CASPT2(13,13) levels. The triangular isomers required a smaller active space (CASPT2(4,8), CASPT2(5,8) and CASPT2(6,8)) due to their lower symmetry which breaks the degeneracy of the π orbitals (see Computational details).

ThS_2^{2+} isomer pair

We begin with the simplest system, η^2-ThS_2^{2+}, where the most plausible bonding scenarios are the binding of two Th^{2+} + $(^3X)S_2^{\bullet\bullet}$ fragments resulting in a triplet state, or alternatively a closed shell molecule partitioned as Th^{4+} + S_2^{2-} (persulphide), in view of the significant stability of the +4 oxidation state of Th.[1] A CASPT2(2,2) optimization for the ground-state singlet and triplet were performed and the resulting energy differences unequivocally favour a closed shell singlet. The triplet is 29.7 kcal mol^{-1} higher in energy and consists of a singly occupied π* MO from the di-sulfide unit plus one $6d_{z^2}$ orbital holding the remaining electron. A re-optimised structure with the MP2 method provides a geometry which is very close to the one obtained with CASPT2(2,2) and with identical reference weights (0.8) in the perturbed wavefunction confirming the lack of multi-reference character of the ground-state singlet (which is 98.7% mono-determinantal). The calculated CASPT2(2,2) equilibrium distances of the ground state are *d*(Th–S) = 2.477 Å and *d*(S–S) = 2.173 Å and those with MP2 *d*(Th–S) = 2.480 Å and *d*(S–S) = 2.169 Å. For comparative purposes a single point evaluation using the CASPT2(10,13) method was used and the linearization energy evaluated to be +59.4 kcal mol^{-1}. The analogous MP2 calculation as expected provided a very similar energy (56.2 kcal mol^{-1}).

US_2^{2+} isomer pair

For the η^2-US_2^{2+} system the most suitable active space was found to be the seven 5f orbitals plus the out of plane π_1^- ($2p_\pi \pm 2p_\pi$) linear combination set of the S_2 fragment (Fig. 3). The lowest singlet, triplet and quintet states were optimised at the CAS(4,8)PT2 level. The results are summarised in Table 2. One of the more interesting aspects is the low energy value of the quintet state with respect to the ground-state triplet which had already been an important conclusion in a preceding paper.[18] This quintet state can be described as a $U^{3+}(5f^3)$ + $S_2^{-\bullet}$ ferromagnetic interaction as evidenced by the natural orbital occupancies (NOOs). The $5f_{\delta 1}$ and the π^- MOs do not mix as in the lower spin states as these MOs remain localised.

In the triplet ground state there is some mixing between the $5f_{\delta 1}$ and the π^- orbital from sulphur. The CI coefficients of the CASPT2(4,8) first order wavefunction show a strong multi-reference character: triplet state has the leading (30%) configuration $^3\varphi_1$ = $\{(5f_\sigma)^\uparrow\ (5f_{\pi 1})^0\ (5f_{\pi 2})^0\ (5f_{\delta 1} + \pi_1^-)^2\ (5f_{\delta 2})^0\ (5f_{\phi 1})^\uparrow\ (5f_{\phi 2})^0\ (5f_{\delta 1} - \pi_1^-)^0\}$ followed by the configuration state function (CSF) with an additional open shell 23% $^3\varphi_2$ = $\{(5f_\sigma)^\uparrow\ (5f_{\pi 1})^0\ (5f_{\pi 2})^0\ (5f_{\delta 1} + \pi_1^-)^\uparrow\ (5f_{\delta 2})^0\ (5f_{\phi 1})^\downarrow\ (5f_{\phi 2})^0\ (5f_{\delta 1} - \pi_1^-)^\uparrow\}$ and 8% $^3\varphi_3$ = $\{(5f_\sigma)^\downarrow\ (5f_{\pi 1})^0\ (5f_{\pi 2})^0\ (5f_{\delta 1} + \pi_1^-)^\uparrow\ (5f_{\delta 2})^0\ (5f_{\phi 1})^\uparrow\ (5f_{\phi 2})^0\ (5f_{\delta 1} - \pi_1^-)^\uparrow\}$. The makeup of the $^3\varphi_2$ CSF is two determinantal: $1/2|(5f_{\delta 1}\ \pi_1^-)^\uparrow\ (5f_{\phi 1})^\downarrow| - 1/2|(5f_{\delta 1} + \pi_1^-)^\downarrow(5f_{\phi 1})^\uparrow|$ where the minus sign shows that this is the M_s = +1 component of the $|S = 1; S_1 = 3/2; S_2 = 1/2\rangle$ coupled state rather than from $|S = 2; S_1 = 3/2; S_2 = 1/2\rangle$. The natural spin density of the unperturbed CAS wavefunction, shown in Fig. 4, highlights the spin coupling at the different An(5f) and π^- sites.

The singlet state is 16.2 kcal mol^{-1} higher in energy and presents a complex electronic structure. Its leading configuration (34%) is $^1\varphi_1$ = $\{(5f_\sigma)^\uparrow\ (5f_{\pi 1})^0\ (5f_{\pi 2})^0\ (5f_{\delta 1} + \pi_1^-)^2\ (5f_{\delta 2})^0\ (5f_{\phi 1})^0\ (5f_{\phi 2})^\downarrow\ (5f_{\delta 1} - \pi_1^-)^0\}$ followed by $^1\varphi_2$ = $\{(5f_\sigma)^\uparrow\ (5f_{\pi 1})^0\ (5f_{\pi 2})^0\ (5f_{\delta 1} + \pi_1^-)^0\ (5f_{\delta 2})^0\ (5f_{\phi 1})^0\ (5f_{\phi 2})^\downarrow\ (5f_{\delta 1} - \pi_1^-)^2\}$ (14%) admixed with several other configurations each below 10% in overall weight.

Table 2 Energies, bond distances and NOOs of the optimised η^2-US_2^{2+} species in several spin states

Total spin	0	1	2
ΔE/(kcal mol^{-1})	+16.2	0	+2.8
d(U–S)/Å	2.577	2.599	2.630
d(S–S)/Å	2.060	2.055	2.049
Natural orbital occupations (NOOs)			
$(5f_{\delta 1}+)\ \pi_1^-$	1.160	1.110	0.988[a]
$5f_\sigma$	0.676	0.910	0.030
$5f_{\phi 1}$	0.645	0.788	0.223
$5f_{\pi 1}$	0.173	0.084	0.888
$5f_{\phi 2}$	0.196	0.170	0.767
$5f_{\delta 2}$	0.275	0.205	0.822
$5f_{\delta 1}$ $(-\pi_1^-)$	0.543	0.692	0.171[a]
$5f_{\pi 2}$	0.279	0.016	0.085

[a] Fully localised orbital, orbital in brackets not present.

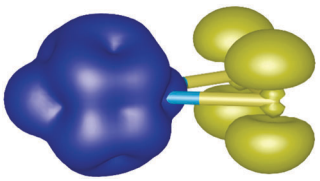

Fig. 4 CASSCF(4,8) spin density plot obtained from the natural spin orbitals of the calculated ^{3}X state of η^2-US_2^{2+}. Positive spin density is blue, negative spin density is yellow.

The non-integer orbital occupations are a consequence of the near degeneracy of one or more states that is present in these highly symmetric systems, specifically the 5f orbitals that are degenerate. A multi-state analysis would resolve all these states but a spectroscopic analysis is beyond the scope of this work.

Both the triplet and singlet states have a $5f_{\delta 1} + \pi_1^-$ MO composition that is approximately 11% $5f_{\delta 2}$ + 89% π_1^- (S) whereas its anti-bonding counterpart $5f_{\delta 1} - \pi_1^-$ is 87% 5f + 14% π^- (S) (see ESI†). Performing a 2 × 2 rotation of the $5f_{\delta 1} \pm \pi_1^-$ orbital pair yields the orthogonal localised $5f_{\delta 1}$ and π_1^- MO pair, which have the occupation numbers of 0.08 and 1.12 respectively. Both these spin states show evidence of exhibiting a side-on $S_2^{-\bullet}$ radical fragment which gradually donates some electronic density as the spin state gets higher. In the quintet state, as seen from Table 2, the (localised) π_1^- MO will lower its NOO to 0.988 involving an approximate back-donation increase of 0.13 e^- from the triplet to the quintet.

From an orbital interaction perspective, the most important interactions in η^2-US_2^{2+} are between the antibonding π_1^- and π_2^- set of di-sulphur and their linear combination with the 5f and 6d functions of uranium (Scheme 1).

Given that the 6d + π_2^- MO is in the inactive group of orbitals its NOO is precisely 2.0. The Mayer–Mulliken[43,44] bond order is a quantitative measure of a bond strength and will be used in this work to assess these magnitudes and serve to compare the compounds under analysis. The U–S bond order calculated from the CASPT2(4,8) density in the ^{3}X state is 0.997 while the S–S bond has a value of 1.078.

Some notable aspects emerge when comparing the bonding scenario with the analogous η^2-UO_2^{2+} species to help understand the preference of the uranyl cation for linearity and the thiolated uranium cations for the chelated form. To this aim we also optimised the triplet η^2-UO_2^{2+} geometry, which lies 5 kcal mol^{-1} below the quintet state, and performed a comparative orbital analysis. Owing to the shorter O–O distance, the 6d/π_2^- overlap and back-donation is not as effective in η^2-UO_2^{2+}. This becomes apparent from the analysis of the relevant MO compositions in both systems. Whereas in η^2-US_2^{2+} the natural orbital is composed of the following atomic orbitals:

$$\Psi_{PT2}(6d + \pi_2^-) = 0.135\phi_U(6p_\pi) + 0.366\phi_U(6d_\pi) + 0.599\phi_{S1}(3p) - 0.598\phi_{S2}(3p) + \ldots$$

in η^2-UO_2^{2+} the 6d contribution decreases while the oxygen 2p orbitals have a slightly higher contribution:

$$\Psi_{PT2}(6d + \pi_2^-) = 0.270\phi_U(6p_\pi) + 0.269\phi_U(6d_\pi) + 0.661\phi_{O1}(2p) - 0.691\phi_{O2}(2p) + \ldots$$

where the $6p_\pi$ orbital in uranium though filled is more accessible to overlap with the π_2^- group MO.

Two important points from this analysis of the η^2-US_2^{2+} and η^2-UO_2^{2+} cations become evident: (1) a σ type of overlap between the 6d orbital with the π_2^- MOs (as shown in Scheme 1) is energetically more stabilising than it would be in a linear $[SUS]^{2+}$ species since the corresponding 6d/3p overlap would then only have π symmetry; (2) U–O bonds are not stable in a side-on arrangement since the 6d orbitals can never have a significant overlap with the 2p set because of the electronegativity of the oxygen atoms.

The NOOs in the $5f_{\delta 1} \pm \pi^-$ set do not change to a significant extent between η^2-UO_2^{2+} and η^2-US_2^{2+} and neither does their composition ($5f_{\delta 1} + \pi_1^-$ = 25% $5f_{\delta 1}$ + 75% π_1^-; $5f_{\delta 1} - \pi_1^-$ = 65% $5f_{\delta 1}$ + 35% π_1^-). The Mayer–Mulliken CASPT2 bond orders are 0.67 for U–O and 0.96 for O–O. The U–O bond is indubitably weaker than that of U–S in these chelates.

The closed shell $[SUS]^{2+}$ species affords no special difficulty in its computational treatment. The calculated U–S equilibrium bond length is 2.193 Å (Table 3) and the (S–U–S) angle is precisely 180°. The CASPT2(12,13) electronic energy difference of linear $[SUS]^{2+}$ with respect to the di-hapto species

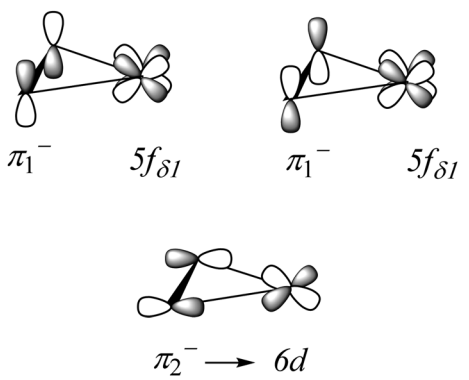

Scheme 1 Main orbital interactions in η^2-AnS_2^{2+}.

Table 3 NOOs and single point energy of the closed shell linear $[SUS]^{2+}$ with respect to the ^{3}X ground state of η^2-US_2^{2+}

ΔE/(kcal mol^{-1})	+8.4
d(U–S)/Å	2.193
NOOs	
$5f_\sigma + \sigma^-$	1.855
σ^+	1.936
π_1^-	1.948
π_2^-	1.948
$5f_{\pi 1} + \pi_1^+$	1.882
$5f_{\pi 2} + \pi_2^+$	1.882
$5f_{\delta 1}$	0.021
$5f_{\delta 2}$	0.014
$5f_{\phi 1}$	0.004
$5f_{\phi 2}$	0.004
$5f_{\pi 1} - \pi_1^+$	0.095
$5f_{\pi 2} - \pi_2^+$	0.095
$5f_\sigma - \sigma^-$	0.106

Table 4 Energies, bond distances and NOOs of the optimised di-haptic neptunium disulphide species [CASPT2(5,8)] in several spin states

Total spin	1/2	3/2	5/2
ΔE/(kcal mol^{-1})	+29.8	0	+3.4
d(Np–S)/Å	2.579	2.580	2.602
d(S–S)/Å	2.054	2.051	2.045
NOOs			
$(5f_{\delta 1}+)\ \pi_1^-$	1.044	1.137	1.000[a]
$5f_\sigma$	0.632	0.926	0.929
$5f_{\phi 1}$	0.575	0.961	0.965
$5f_{\pi 1}$	0.501	0.116	0.928
$5f_{\phi 2}$	0.632	0.131	0.064
$5f_{\delta 2}$	0.592	0.867	0.929
$5f_{\delta 1}\ (-\pi_1^-)$	0.575	0.786	0.080[a]
$5f_{\pi 2}$	0.450	0.077	0.106

[a] Fully localised orbital, orbital in brackets not present.

is +8.4 kcal mol^{-1}, a comparatively smaller figure than the previous[18] DFT value of +40.9 kcal mol^{-1}.

NpS_2^{2+} isomer pair

With the neptunium system an analogous chemical bonding picture emerges (Table 4), the only difference being the electron count. The ground state is a quadruplet (^{4}X), the sextet state is located slightly higher in energy (3.4 kcal mol^{-1}) with respect to the triplet-quintet gap (2.8 kcal mol^{-1}) in η^2-US_2^{2+}. In the sextet state the $5f_{\delta 1}$ orbital also does not mix with the π_1^- group MO which leads to a ferromagnetic $Np^{3+}(5f^4)$ + $S_2^{-\bullet}$ coupling analogously to the η^2-US_2^{2+} quintet state.

Upon orbital localisation of the ^{4}X CASPT2(5,8) wavefunction the occupation numbers of the two $5f_{\delta 1}$ and π_1^- orbitals are 0.120 and 1.12 respectively, values similar to the ones previously obtained for the η^2-US_2^{2+} cation. Indeed, the only significant change with respect to the η^2-US_2^{2+} species is that there is one additional electron in the $5f_{\delta 2}$ atomic orbital: 34% $^4\varphi_1 = \{(5f_\sigma)^\uparrow\ (5f_{\pi 1})^0\ (5f_{\pi 2})^0\ (5f_{\delta 1} + \pi_1^-)^2\ (5f_{\delta 2})^\uparrow\ (5f_{\phi 1})^\uparrow\ (5f_{\phi 2})^0\ (5f_{\delta 1} - \pi_1^-)^0\}$ and 18% $^4\varphi_2 = \{(5f_\sigma)^\uparrow\ (5f_{\pi 1})^0\ (5f_{\pi 2})^0\ (5f_{\delta 1} + \pi_1^-)^\uparrow\ (5f_{\delta 2})^\uparrow\ (5f_{\phi 1})^\downarrow\ (5f_{\phi 2})^0\ (5f_{\delta 1} - \pi_1^-)^0\}$ which is entirely analogous to the $^3\varphi_2$ CSF in η^2-US_2^{2+}. This spin coupling can be demonstrated by the CASSCF natural spin density shown in Fig. 5.

Since nothing is known about the linear $[SNpS]^{2+}$ structure a survey of the most chemically intuitive spin states was undertaken (Table 5). The lowest energy micro-state is also a quartet but situated some +31.8 kcal mol^{-1} above the ground state of η^2-NpS_2^{2+}. This linear structure has an equilibrium distance of 2.256 Å and the (S–Np–S) angle is very close to 180°.

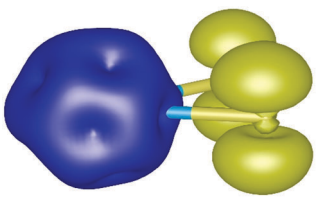

Fig. 5 CASSCF(5,8) spin density plot obtained from the natural spin orbitals of the ^{4}X state of η^2-NpS_2^{2+}. Positive spin density is blue, negative spin density is yellow.

Table 5 NOOs, bond distances and optimised energies [CASPT2(13,13)] of linear NpS_2^{2+} with respect to the ^{4}X ground state

Total spin	1/2	3/2
ΔE/(kcal mol^{-1})	+3.5	0
d(Np–S)/Å	2.265	2.256
NOOs		
$5f_\sigma + \sigma^-$	1.856	0.999
σ^+	1.958	1.873
π_1^-	1.968	1.972
π_2^-	1.968	1.972
$5f_{\pi 1} + \pi_1^+$	1.859	1.872
$5f_{\pi 2} + \pi_2^+$	1.859	1.872
$5f_{\delta 1}$	0.0200	0.502
$5f_{\delta 2}$	0.0200	0.502
$5f_{\phi 1}$	0.0048	0.501
$5f_{\phi 2}$	0.996	0.501
$5f_{\pi 1} - \pi_1^+$	0.169	0.156
$5f_{\pi 2} - \pi_2^+$	0.169	0.156
$5f_\sigma - \sigma^-$	0.158	0.129

The Mayer–Mulliken Np–S CASPT2(13,13) bond order of the linear $[SNpS]^{2+}$ molecule has the value of 2.077 which is less than in the corresponding uranium system (2.485). This is due to the higher NOO count of the $5f_{\pi 1} - \pi_1^+/5f_{\pi 2} - \pi_2^+$ anti-bonding MOs (Fig. 6).

A single point run of the optimised ground state geometries under C_{2v} symmetry reveals that the ground state structure of the triangular isomer has triply degenerate quartet states $^4A_1$,$^4A_2$,$^4B_2$ (see ESI†) corresponding to the occupation of non-bonding 5f orbitals in a different symmetry species and equal energy. The ground state of the linear species is doubly degenerate with $^4A_1$,$^4B_1$ states having equal energy, which in $D_{\infty h}$ symmetry will correspond to a doubly degenerate state term symbol (Π, Δ, Φ...).

PuS_2^{2+} isomer pair

We focus now on the analysis of the isomers of the PuS_2^{2+} dication. The ground state of the η^2-PuS_2^{2+} species is a quintet. This state comes as a natural extension of the electronic structure seen in η^2-US_2^{2+} and η^2-NpS_2^{2+} (triplet and quartet, respectively). The difference now is that little di-radical coupling is present between the π antibonding MOs in di-sulphur and the remainder of the 5f manifold. This ground state is more complex in its configurational make-up than has been described heretofore. The leading CASPT2 CSF is $^5\varphi_1 = \{(5f_\sigma)^\uparrow\ (5f_{\pi 1})^0\ (5f_{\pi 2})^0\ (5f_{\delta 1} + \pi_1^-)^2\ (5f_{\delta 2})^\uparrow\ (5f_{\phi 1})^\uparrow\ (5f_{\phi 2})^\uparrow\ (5f_{\delta 1} - \pi_1^-)^0\}$ (27.5%) followed by $^5\varphi_2 = \{(5f_\sigma)^\uparrow\ (5f_{\pi 1})^0\ (5f_{\pi 2})^0\ (5f_{\delta 1} + \pi_1^-)^\uparrow\ (5f_{\delta 2})^\downarrow\ (5f_{\phi 1})^\uparrow\ (5f_{\phi 2})^\uparrow\ (5f_{\delta 1} - \pi_1^-)^\uparrow\}$ (16.0%) and $^5\varphi_3 = \{(5f_\sigma)^\uparrow\ (5f_{\pi 1})^0\ (5f_{\pi 2})^0\ (5f_{\delta 1} + \pi_1^-)^0\ (5f_{\delta 2})^\uparrow\ (5f_{\phi 1})^\uparrow\ (5f_{\phi 2})^\uparrow\ (5f_{\delta 1} - \pi_1^-)^2\}$ (15.7%), as well as the spin coupled di-radical which is now a minority $^5\varphi_4 = \{(5f_\sigma)^\uparrow\ (5f_{\pi 1})^0\ (5f_{\pi 2})^0\ (5f_{\delta 1} + \pi_1^-)^\uparrow\ (5f_{\delta 2})^\uparrow\ (5f_{\phi 1})^\uparrow\ (5f_{\phi 2})^\uparrow\ (5f_{\delta 1} - \pi_1^-)^\downarrow\}$ (10.5%). The respective spin density of the unperturbed wavefunction is displayed in Fig. 7.

The energy of the lower spin states is much higher, 44 and 66 kcal mol^{-1} above the ground state for the triplet and singlet (Table 6), respectively.

Analogously to the η^2-US_2^{2+} cation, a low lying higher spin state exists in the form of a septet which is pratically

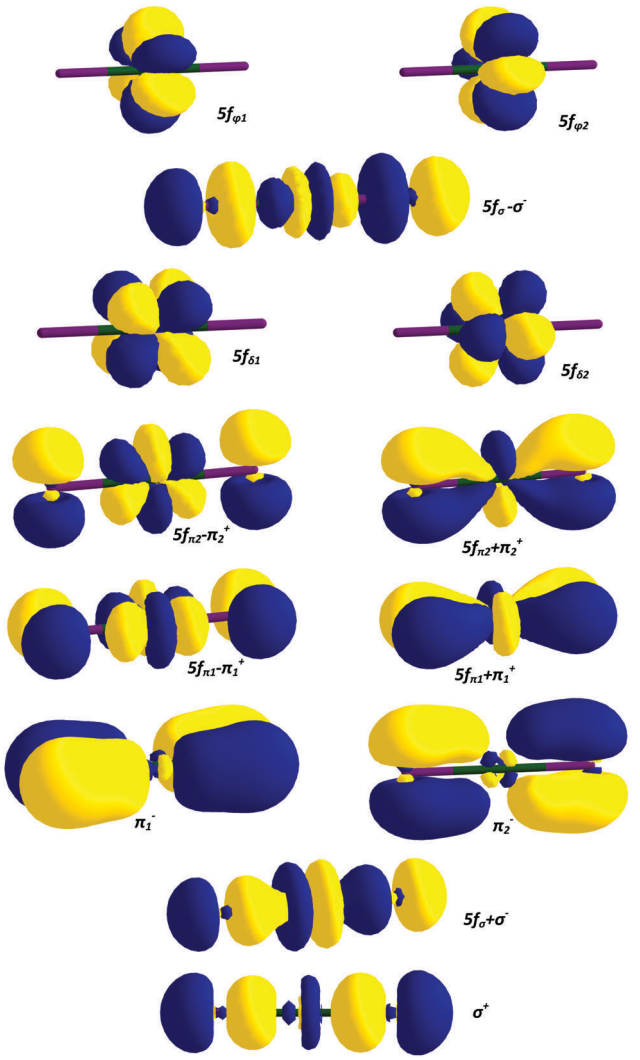

Fig. 6 Active space orbitals used in the optimisation of the linear isomers such as NpS_2^{2+}.

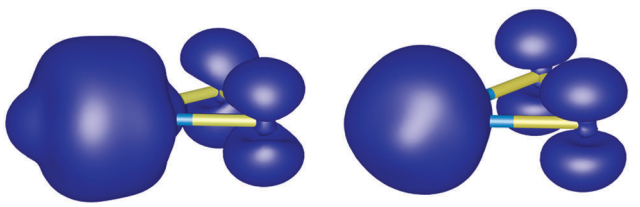

Fig. 7 CASSCF(6,8) spin density plots obtained from the natural spin orbitals of the ^{5}X (left) and ^{7}X states (right) of η^2-PuS_2^{2+}.

degenerate, only 0.7 kcal mol^{-1} above the energy of the quintet. The majority contribution stems from the $^7\varphi_1 = \{(5f_\sigma)^\uparrow\ (5f_{\pi 1})^\uparrow\ (5f_{\pi 2})^0\ (5f_{\delta 1})^0\ (5f_{\delta 2})^\uparrow\ (5f_{\phi 1})^\uparrow\ (5f_{\phi 2})^\uparrow\ (\pi_1^-)^\uparrow\}$ (63%) configuration state function and trailing below it in predominance is $^7\varphi_2 = \{(5f_\sigma)^0\ (5f_{\pi 1})^0\ (5f_{\pi 2})^\uparrow\ (5f_{\delta 1})^\uparrow\ (5f_{\delta 2})^\uparrow\ (5f_{\phi 1})^\uparrow\ (5f_{\phi 2})^\uparrow\ (\pi_1^-)^\uparrow\}$ (37%) where now the $5f_{\delta 1}$ orbitals do not mix as seen in the highest spin states of the previous disulphides.

The linear $[SPuS]^{2+}$ dication has also never been addressed computationally so three spin states S = 0, 1 and 2 were optimised to ascertain the nature of its ground state and compare it to the triangular species in the extended active space. Although the linear species tend to have lower spin states due to the An≡S triple bonds, in the case of plutonium this is no longer the case since the $5f_\sigma + \sigma^-$ MO becomes partially occupied just as it was seen in $[SNpS]^{2+}$ and three other 5f orbitals are singly occupied (Table 7). The triplet state is doubly degenerate under C_{2v} symmetry ($^3A_2 + {}^3B_2$, see ESI†) and is 1.8 kcal mol^{-1} higher in energy and quasi-degenerate with the quintet state ($^5A_2$). The latter resolution into a single state explains why the latter NOOs are close to either 0, 1 or 2.

Table 6 Energies, NOOs and bond distances of the optimised di-haptic plutonium disulphide species [CASPT2(6,8)] in several spin states

Total spin	0	1	2	3
ΔE/(kcal mol^{-1})	+66.1	+44.3	0	+0.7
d(Pu–S)/Å	2.552	2.559	2.570	2.581
d(S–S)/Å	2.050	2.047	2.050	2.041
NOOs				
$(5f_{\delta 1}) + \pi^-$	1.218	1.097	1.073	0.988[a]
$5f_\sigma$	1.101	0.862	0.988	0.629
$5f_{\phi 1}$	0.735	0.971	0.988	0.988
$5f_{\pi 1}$	0.534	0.176	0.145	0.629
$5f_{\phi 2}$	0.749	0.331	0.988	0.988
$5f_{\delta 2}$	0.605	1.582	0.850	0.988
$5f_{\delta 1}$ $(-\pi^-)$	0.872	0.729	0.765	0.365[a]
$5f_{\pi 2}$	0.122	0.192	0.145	0.365

[a] Localised orbital, orbital in brackets not participating.

Table 7 NOOs, bond distances and optimised energies [CASPT2(14,13)] of linear PuS_2^{2+} with respect to the ^{5}X ground state

Total spin	0	1	2
ΔE/(kcal mol^{-1})	+32.8	+1.8	0
d(Pu–S)/Å	2.301	2.279	2.279
NOOs			
$5f_\sigma + \sigma^-$	1.806	1.793	0.984
σ^+	1.903	1.908	1.817
π_1^-	1.917	1.904	1.921
π_2^-	1.917	1.904	1.925
$5f_{\pi 1} + \pi_1^+$	1.798	1.748	1.784
$5f_{\pi 2} + \pi_2^+$	1.802	1.748	1.791
$5f_{\delta 1}$	0.419	0.501	0.978
$5f_{\delta 2}$	0.048	0.506	0.978
$5f_{\phi 1}$	1.525	0.492	0.982
$5f_{\phi 2}$	0.016	0.497	0.007
$5f_{\pi 1} - \pi_1^+$	0.209	0.276	0.220
$5f_{\pi 2} - \pi_2^+$	0.208	0.276	0.222
$5f_\sigma - \sigma^-$	0.190	0.209	0.158

Global view

The most significant conclusion of these calculations is that the thermodynamic energy for the linearization process increases fourfold upon changing from U to Pu (Table 8). Presumably this trend will be more pronounced for the later actinides since orbital mixing is expected to take on a greater role.[20] Additionally, the depopulation of an An–S σ bond in the linear species is already present in the Np and Pu sulfides. This finding

Table 8 Summary of single point CASPT2 energies (in kcal mol^{-1}) and ground states for all the actinide disulphides contrasted with the uranyl cation

CASPT2(n,13)	Linear	Triangular
ThS_2^{2+}, n = 10	+59.4 (S = 0)	0 (S = 0)
US_2^{2+}, n = 12	+8.4 (S = 0)	0 (S = 1)
NpS_2^{2+}, n = 13	+31.8 (S = 3/2)	0 (S = 3/2)
PuS_2^{2+}, n = 14	+35.8 (S = 2)	0 (S = 2)
UO_2^{2+}, n = 12	0 (S = 0)	+126.6 (S = 1)

defies conventional chemical intuition such that in the linear structures the π bonds are resilient and σ bonds are weakened. Since σ overlap is no longer as efficient as in the early actinides, a side-on coordination will become energetically more rewarding. From an empirical viewpoint, the decreasing stability of high oxidation states beyond Pu[1] supports this analysis.

To explain the observed trend in the linearization energy two factors must be taken into account: one is the strength of the S–S bonds in the triangular structure *versus* the strength of the An–S bonds in the linear structures. If the former is constant, the latter will dictate the trend in isomer conversion energy. Indeed, a linear correlation can be established between the difference in Mayer bond order between the linear and triangular ground state perturbed densities and the electronic energy differences of the interconversion process (Fig. 8). This is a consequence of the S–S bond strength remaining mostly constant throughout the range of actinide sulphides being examined, with the only exception being thorium for which the weaker S–S bond is compensated by a stronger Th=S double bond. A listing of the calculated MBOs is presented in the ESI.†

As one examines this same interconversion process in the classic uranyl cation ($[OUO]^{2+}$) however it is observed that the energy change is incomparably high. This may not just be due to the change in bond order which is indeed significant (ΔBO = 1.61) but also to the relative instability in the formation of a single O–O bond in the triangular species with respect to the S–S one in η^2-AnS_2^{2+}. The dissociation energy of the O–O bond in H_2O_2 is ΔH_{diss} = 49.5 kcal mol^{-1} whereas for the S–S one (H_2S_2) it is ΔH_{diss} = 62.6 kcal mol^{-1},[39] meaning that a single S–S bond is stronger than a single O–O bond. On this basis there is an additional incentive for the uranyl species to remain linear.

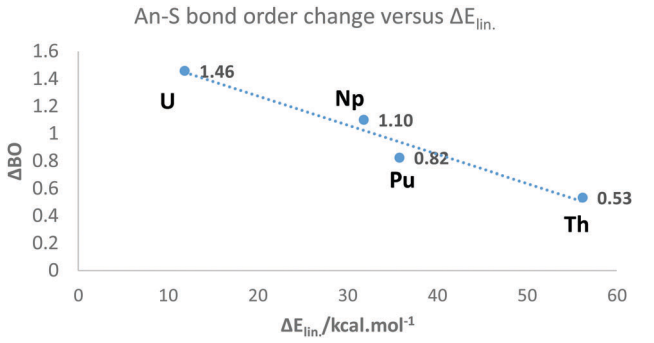

Fig. 8 Difference in An–S Mayer–Mulliken bond order between the linear and the triangular structures taken as a function of the isomer conversion energy.

As reported above, the polysulphides ThS_3^+, NpS_3^+ and ThS_4^+ were also synthesized by sequential abstractions of S atoms from COS. Although these species were not calculated, it is reasonable to surmise regarding possible structures. The computed structures of US_3^{2+} and US_4^{2+} were reported in ref. 18. Given that these previous DFT calculations predicted the same triangular triplet structure for US_2^{2+} as was computed at the higher level of theory employed here, it is expected that the previously computed ground state structures for US_3^{2+} and US_4^{2+} are also valid; both are triplet, with the former having one η^2-coordinated S_3 moiety, and the latter having two η^2-coordinated S_2 moieties. It is surmised that the structures of ThS_3^{2+} and NpS_3^{2+} similarly have an S_3 moiety that is η^2-coordinated to the metal center. The proposed ground state structures for ThS_3^{2+} and NpS_3^{2+} might be accessible from the ground state structures of the disulphides *via* insertion of an S atom into an An–S or S–S bond; both insertions likely present substantial barriers such that the experimentally produced trisulphides may not exhibit the lowest energy structures. It should be remarked that formation of triangular AnS_2^{2+} from AnS^{2+} by addition of an S atom does not require An–S or S–S bond cleavage and should thus present a substantially lower, perhaps negligible, kinetic barrier. The structure of ThS_4^{2+} may be analogous to the $[(\eta^2\text{-}S_2)U(\eta^2\text{-}S_2)]^{2+}$ structure reported in ref. 18, although the alternative $[(\eta^2\text{-}S_4)Th]^{2+}$ structure cannot be excluded. The triplet spin state of US_4^{2+} suggests a formally U^{4+} oxidation state but the U–S bond distances indicate four U–S single bonds and a potentially higher oxidation state, which is inaccessible in the case of Th for which the tetravalent oxidation state is realistically the highest. As with the trisulphides, formation of tetrasulphides by S atom addition may present sufficiently high barriers that the structure obtained under low-energy experimental conditions is not necessarily the computed ground state structure.

Conclusions

The gas-phase synthesis of new actinide disulphide dications, AnS_2^{2+} (An = Th, Np), was accomplished by sequential reactions of An^{2+} ions with COS; for An = Pu and Am, An^{2+} ions were unreactive. CASPT2 computations were performed to assess the structures and bonding of the new AnS_2^{2+} ions (An = Th, Np), of PuS_2^{2+} to uncover trends along the An series, and of US_2^{2+}, previously studied experimentally and examined by DFT. These computations revealed that, like in the case of uranium, the AnS_2^{2+} ions have ground-state structures of the metallacycle type, with the presence of a persulphide ligand in η^2-ThS_2^{2+}, formally corresponding to a Th(IV) species, and of supersulphide ligands in US_2^{2+}, NpS_2^{2+}, and PuS_2^{2+}, formally corresponding to An(III) species. Molecular orbital and energetic analysis of the dicationic species reveal that the existence of linear actinide di-chalcogenides are likely confined to the uranyl (OUO^{2+})

species due to three factors: the destabilising effect that the poor 2p → 6d donating ability exacts upon the system with side-on coordination (η^2-UO_2^{2+}), the stronger σ bond present in supersulphide ($S_2^{-\bullet}$) stabilising the triangular species with respect to the linear isomer and finally the depopulation of the $5f_\sigma + \sigma^-$ bonding orbitals in the ground states of the $[SAnS]^{2+}$ species which weaken the strength of this interaction and de-stabilise the linear isomers.

The An(IV/III) reduction potentials clearly indicate a significant stability of Th(IV) species and an increasing relative stability of the An(III) when moving from U to Pu, culminating in a clear predominance of Am(III).[1] Linear thioactinyl structures are higher in energy, with a difference that increases fourfold upon changing from U to Pu. An inverse correlation was found concerning the difference in the An–S bond order between linear and triangular structures and the linearization energy, showing that the di-sulphide side-on coordination gains strength thus stabilising the triangular isomers with heavier actinides.

Acknowledgements

This work was supported by: Fundação para a Ciência e a Tecnologia (Portugal) through research contract UID/Multi/04349/2013, PhD grant SFRH/BD/70475/2010 to A. F. L., post-doc grant SFRH/BPD/110419/2015 and PTDC/QEQ-QIN/3414/2014 project grant to N. A. G. B., Ciência 2007 Programme, and RNEM-Portuguese Mass Spectrometry Network; Spanish Ministerio de Economia y Competitividad (MINECO) through research contract CTQ2014-52824-R; and U.S. Department of Energy, Office of Basic Energy Sciences, Heavy Element Chemistry, at LBNL under Contract DE-AC02-05CH11231. The COS was a generous gift from Dr João M. A. Frazão at ISEL, Lisbon, Portugal.

References

1 N. M. Edelstein, J. Fuger, J. J. Katz and L. R. Morss, in *The Chemistry of the Actinide and Transactinide Elements*, ed. L. R. Morss, N. M. Edelstein and J. Fuger, Springer, Dordrecht, The Netherlands, 4th edn, 2010, vol. 3, pp. 1753–1835.
2 R. J. Baker, *Chem. – Eur. J.*, 2012, **18**, 16258–16271.
3 K.-X. Wang and J.-S. Chen, *Acc. Chem. Res.*, 2011, **44**, 531–540.
4 J. Qiu and P. C. Burns, *Chem. Rev.*, 2013, **113**, 1097–1120.
5 M. B. Andrews and C. L. Cahill, *Chem. Rev.*, 2013, **113**, 1121–1136.
6 R. G. Denning, *J. Phys. Chem. A*, 2007, **111**, 4125–4143.
7 M. Buhl and G. Wipff, *ChemPhysChem*, 2011, **12**, 3095–3105.
8 D. Wang, W. F. van Gunsteren and Z. Chai, *Chem. Soc. Rev.*, 2012, **41**, 5836–5865.
9 A. Kovacs, R. J. Konings, J. K. Gibson, I. Infante and L. Gagliardi, *Chem. Rev.*, 2015, **115**, 1725–1759.
10 N. Kaltsoyannis, P. J. Hay, J. Li, J.-P. Blaudeau and B. E. Bursten, in *The Chemistry of the Actinide and Transactinide Elements*, ed. L. R. Morss, N. M. Edelstein and J. Fuger, Springer, Dordrecht, The Netherlands, 4th edn, 2010, vol. 3, pp. 1893–2012.
11 T. W. Hayton, *Chem. Commun.*, 2013, **49**, 2956–2973.
12 H. S. La Pierre and K. Meyer, *Inorg. Chem.*, 2013, **52**, 529–539.
13 M. B. Jones and A. J. Gaunt, *Chem. Rev.*, 2013, **113**, 1137–1198.
14 M. Ephritikhine, *Coord. Chem. Rev.*, 2016, **319**, 35–62.
15 S. T. Liddle, *Angew. Chem., Int. Ed.*, 2015, **54**, 8604–8641.
16 J. L. Brown, E. R. Batista, J. M. Boncella, A. J. Gaunt, S. D. Reilly, B. L. Scott and N. C. Tomson, *J. Am. Chem. Soc.*, 2015, **137**, 9583–9586.
17 J. L. Brown, S. Fortier, G. Wu, N. Kaltsoyannis and T. W. Hayton, *J. Am. Chem. Soc.*, 2013, **135**, 5352–5355.
18 C. C. L. Pereira, M. d. C. Michelini, J. Marçalo, Y. Gong and J. K. Gibson, *Inorg. Chem.*, 2013, **52**, 14162–14167.
19 M. L. Neidig, D. L. Clark and R. L. Martin, *Coord. Chem. Rev.*, 2013, **257**, 394–406.
20 N. Kaltsoyannis, *Inorg. Chem.*, 2013, **52**, 3407–3413.
21 N. Kaltsoyannis, *Dalton Trans.*, 2016, **45**, 3158–3162.
22 P. D. Dau, R. E. Wilson and J. K. Gibson, *Inorg. Chem.*, 2015, **54**, 7474–7480.
23 B. Liang and L. Andrews, *J. Phys. Chem. A*, 2002, **106**, 4038–4041.
24 B. Liang, L. Andrews, N. Ismail and C. J. Marsden, *Inorg. Chem.*, 2002, **41**, 2811–2813.
25 L. Andrews, X. Wang, B. Liang, F. Ruipérez, I. Infante, A. D. Raw and J. A. Ibers, *Eur. J. Inorg. Chem.*, 2011, 4457–4463.
26 C. C. L. Pereira, C. J. Marsden, J. Marçalo and J. K. Gibson, *Phys. Chem. Chem. Phys.*, 2011, **13**, 12940–12958.
27 J. K. Gibson, *J. Mass Spectrom.*, 1999, **34**, 1166–1177.
28 B. O. Roos, in *Adv. Chem. Phys.*, ed. K. P. Lawley, John Wiley & Sons, Inc., 1987, vol. 69, pp. 399–445.
29 R. Shepard, in *Adv. Chem. Phys.*, ed. K. P. Lawley, John Wiley & Sons, Inc., 1987, vol. 69, pp. 63–200.
30 F. Aquilante, J. Autschbach, R. K. Carlson, L. F. Chibotaru, M. G. Delcey, L. De Vico, I. F. Galvan, N. Ferre, L. M. Frutos, L. Gagliardi, M. Garavelli, A. Giussani, C. E. Hoyer, G. Li Manni, H. Lischka, D. X. Ma, P. A. Malmqvist, T. Muller, A. Nenov, M. Olivucci, T. B. Pedersen, D. L. Peng, F. Plasser, B. Pritchard, M. Reiher, I. Rivalta, I. Schapiro, J. Segarra-Marti, M. Stenrup, D. G. Truhlar, L. Ungur, A. Valentini, S. Vancoillie, V. Veryazov, V. P. Vysotskiy, O. Weingart, F. Zapata and R. Lindh, *J. Comput. Chem.*, 2016, **37**, 506–541.
31 J. Almlöf and P. Taylor, *J. Chem. Phys.*, 1987, **86**, 4070–4077.
32 B. O. Roos, R. Lindh, P.-A. Malmqvist, V. Veryazov and P.-O. Widmark, *J. Phys. Chem. A*, 2003, **108**, 2851–2858.
33 B. O. Roos, R. Lindh, P.-A. Malmqvist, V. Veryazov and P.-O. Widmark, *J. Phys. Chem. A*, 2005, **109**, 6575–6579.
34 P. O. Widmark, P. A. Malmqvist and B. Roos, *Theor. Chim. Acta*, 1990, **77**, 291–306.
35 B. A. Heß, C. M. Marian, U. Wahlgren and O. Gropen, *Chem. Phys. Lett.*, 1996, **251**, 365–371.
36 N. Douglas and N. M. Kroll, *Ann. Phys.*, 1974, **82**, 89–155.

37 G. Jansen and B. A. Hess, *Phys. Rev. A: At., Mol., Opt. Phys.*, 1989, **39**, 6016–6017.
38 F. Aquilante, T. B. Pedersen, R. Lindh, B. O. Roos, A. S. d. Merás and H. Koch, *J. Chem. Phys.*, 2008, **129**, 024113.
39 S. G. Lias, J. E. Bartmess, J. F. Liebman, J. L. Holmes, R. D. Levin and W. G. Mallard, *J. Phys. Chem. Ref. Data, Monogr. Suppl.*, 1988, **17**(1).
40 J. K. Gibson, R. G. Haire, M. Santos, J. Marçalo and A. Pires de Matos, *J. Phys. Chem. A*, 2005, **109**, 2768–2781.
41 J. Marçalo, M. Santos and J. K. Gibson, *Phys. Chem. Chem. Phys.*, 2011, **13**, 18322–18329.
42 J. Marçalo and J. K. Gibson, *J. Phys. Chem. A*, 2009, **113**, 12599–12606.
43 I. Mayer, *Int. J. Quantum Chem.*, 1986, **29**, 73–84.
44 R. S. Mulliken, *J. Chem. Phys.*, 1955, **23**, 1833–1840.